The EMBO Journal (2012) 31, 214–227 | © 2012 European Molecular Biology Organization | Some Rights Reserved 0261-4189/12
www.embojournal.org

THE EMBO JOURNAL

EMBO open

Myosin-5, kinesin-1 and myosin-17 cooperate in secretion of fungal chitin synthase

Martin Schuster[1,4], Steffi Treitschke[1,2,4], Sreedhar Kilaru[1], Justin Molloy[3], Nicholas J Harmer[1] and Gero Steinberg[1,*]

[1]Department of Biosciences, University of Exeter, Exeter, UK, [2]Personalisierte Tumortherapie, Fraunhofer ITEM-R, Regensburg, Germany and [3]MRC National Institute for Medical Research, Mill Hill London, UK

Plant infection by pathogenic fungi requires polarized secretion of enzymes, but little is known about the delivery pathways. Here, we investigate the secretion of cell wall-forming chitin synthases (CHSs) in the corn pathogen *Ustilago maydis*. We show that peripheral filamentous actin (F-actin) and central microtubules (MTs) form independent tracks for CHSs delivery and both cooperate in cell morphogenesis. The enzyme Mcs1, a CHS that contains a myosin-17 motor domain, is travelling along both MTs and F-actin. This transport is independent of kinesin-3, but mediated by kinesin-1 and myosin-5. Arriving vesicles pause beneath the plasma membrane, but only ~15% of them get exocytosed and the majority is returned to the cell centre by the motor dynein. Successful exocytosis at the cell tip and, to a lesser extent at the lateral parts of the cell requires the motor domain of Mcs1, which captures and tethers the vesicles prior to secretion. Consistently, Mcs1-bound vesicles transiently bind F-actin but show no motility *in vitro*. Thus, kinesin-1, myosin-5 and dynein mediate bi-directional motility, whereas myosin-17 introduces a symmetry break that allows polarized secretion.

The EMBO Journal (2012) **31,** 214–227. doi:10.1038/emboj.2011.361; Published online 25 October 2011
Subject Categories: membranes & transport; cell & tissue architecture
Keywords: cytoskeleton; membrane trafficking; molecular motors; plant pathogen

Introduction

In eukaryotes, the cytoskeleton provides filamentous tracks for intracellular motility of cargo, including organelles and vesicles. Membrane trafficking along the secretory pathway is based on filamentous actin (F-actin) and microtubules (MTs; Allan and Schroer, 1999). These filaments are used by membrane transporters, including the ubiquitous MT-based kinesin-1 and the F-actin-dependent myosin-5 to deliver their cargo to polar sites of exocytosis (Vale, 2003). It is generally assumed that both cytoskeletal systems have complementary roles, with MTs and kinesin motors supporting long-range motility, whereas actin and myosin-5 are involved in short-range movement near the plasma membrane (Langford, 1995). In addition to these well-understood motors, eukaryotic cells contain numerous unconventional myosins, which share a myosin-motor domain (MMD) but are thought to have more stationary functions rather than travelling along the actin filament (Woolner and Bement, 2009). Among these motors are the fungal-specific class 17 myosins, which are virulence factors that are required for successful infection of host plants by fungal intruders (Madrid *et al*, 2003; Weber *et al*, 2006; Werner *et al*, 2007). Fungal class 17 myosins consist of a N-terminal MMD fused to a chitin synthase (CHS) region that contains several transmembrane domains by which myosin-17 is thought to bind secretory vesicles (Fujiwara *et al*, 1997; Weber *et al*, 2006). After fusion of these vesicles with the plasma membrane, the CHS region gets exposed and participates in the formation of the fungal cell wall (Munro and Gow, 2001). An intact cell wall protects the fungus from defence reactions of the plant, and it has been shown that fungi are not able to infect their host without myosin-17 in plant and human pathogens (Madrid *et al*, 2003; Liu *et al*, 2004; Weber *et al*, 2006; Werner *et al*, 2007; Treitschke *et al*, 2010). Polar localization of myosin-17 in *Aspergillus nidulans*, *Wangiella dermatitides* and *Ustilago maydis* depends on F-actin (Takeshita *et al*, 2005; Abramczyk *et al*, 2009; Treitschke *et al*, 2010) and fungal myosin-17 binds actin *in vitro* (Takeshita *et al*, 2005). However, the motor domain of Mcs1, the myosin-17 in the corn pathogen *U. maydis* (Weber *et al*, 2006), is not required for its motility (Treitschke *et al*, 2010). Instead, anterograde transport of Mcs1 depends upon both MTs and F-actin (Treitschke *et al*, 2010). These results suggest that F-actin and MTs cooperate in CHS delivery and that the myosin-17 MMD has other roles in secretion.

In this study we focus on two questions: (1) what is the delivery mechanism for CHSs and (2) what is the precise role of the myosin-17 MMD in CHS secretion? We found that the default behaviour of Mcs1-bound membranes is bi-directional motility, which is supported by myosin-5, kinesin-1 and dynein. Most vesicles have a short residence time at the plasma membrane, and only ~15% become docked for several seconds and fuse with the plasma membrane. Apical and lateral secretion of Mcs1 requires its MMD, and our data argue that it serves to capture vesicles at sites of exocytosis by tethering them to cortical actin. Thus, an actin/myosin-5 and an MT/kinesin-1 pathway deliver Mcs1 to the growth region, where its myosin-17 MMD breaks the symmetry of bi-directional transport and fosters polarized exocytosis.

Results

F-actin/myosin-5 and MTs/kinesin-1 provide independent routes for CHS secretion

As a first step towards understanding the role of the cytoskeleton in polarized secretion in *U. maydis*, we set out to

*Corresponding author. Department of Biosciences, University of Exeter, Stocker Road, Exeter EX4 4QD, UK. Tel.: +44 139 226 3476; Fax: +44 139 226 3434; E-mail: G.Steinberg@exeter.ac.uk
[4]These authors contributed equally to this work

Received: 30 March 2011; accepted: 6 September 2011; published online: 25 October 2011

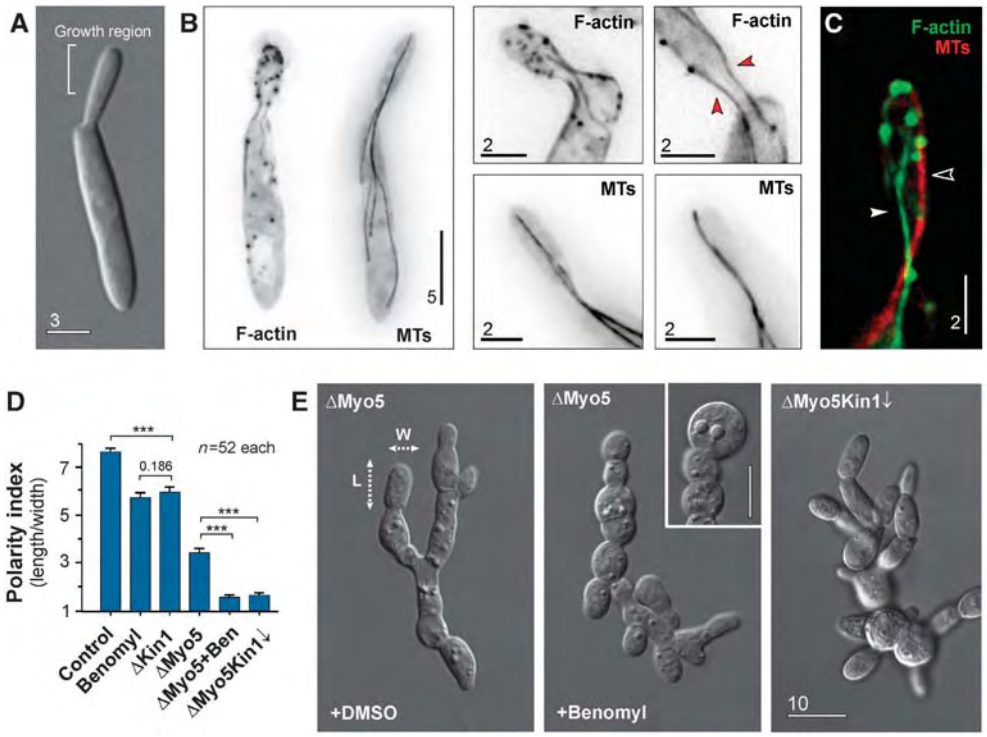

Figure 1 The role of the cytoskeleton in polarized growth of *U. maydis*. (**A**) Organization of yeast-like cells of *U. maydis*. Cells form polar buds that are growing at their tip. Bar represents micrometers. (**B**) The organization of F-actin, labelled with Lifeact-GFP and MTs visualized by GFP-αtubulin. F-actin is found in patches and long cables that localize at the cellular periphery (red arrowheads). MTs are extending far into the mother cell and are positioned more centrally. Images are contrast inverted. Bar represents micrometers. See also Supplementary Movie S1. (**C**) Co-localization of F-actin and MTs. Both filament systems are spatially separated. Bar represents micrometers. (**D**) Bar chart showing the polarity index, which is the quotient of the cell length divided by the cell width (see panel (**E**), dotted arrows, L, length; W, width). Control cells were treated with the solvent DMSO; Benomyl indicates control cells treated with 30 μM of the MT inhibitor Benomyl; ΔKin1 represents a *kin1*-null mutant (Lehmler *et al*, 1997); ΔMyo5 represents a *myo5*-null mutant (Weber *et al*, 2003); ΔMyo5 + Ben indicates *myo5*-null mutants that were treated with 30 μM of the MT inhibitor Benomyl; ΔMyo5Kin1↓ represents a *myo5*-null mutant in which kinesin-1 expression is down-regulated (Schuchardt *et al*, 2005). Statistical significance was tested using an unpaired *t*-test with Welch's correction. Triple asterisk indicates statistical significance at $P<0.0001$. Values are mean ± s.e.m., sample size *n* is given. (**E**) Morphology of *myo5*-null mutants (ΔMyo5), of *myo5*-null mutants after disruption of MTs by Benomyl and *myo5*-null mutants after down-regulation of kinesin-1 (ΔMyo5Kin1↓). Dotted arrow, L, length; dotted arrow W, width of a cell. These dimensions were used to determine the polarity index given in (**D**). Bar represents micrometers.

visualize MTs and F-actin in live cells. Haploid cells of *U. maydis* grow as yeasts that form a daughter bud at one pole (Figure 1A). We used a modified Lifeact-GFP fusion protein (Riedl *et al*, 2008) to visualize F-actin in yeast-like cells of *U. maydis*. Expression of Lifeact-GFP specifically labelled actin patches, which are sites of endocytosis (Kaksonen *et al*, 2003), and decorated F-actin cables (Figure 1B, F-actin). These cables were located at the cell periphery and formed a connection between mother cell and the growing daughter cell (Figure 1B, red arrowheads). In contrast, GFP-αtubulin-labelled MTs were located more centrally and reached far into the growth region (Figure 1B; Supplementary Movie S1; Steinberg *et al*, 2001). To investigate the relationship between the cytoskeletal filament systems, we co-expressed Lifeact-GFP and mCherry-αtubulin. We found that both filament systems are spatially separated (Figure 1C, filled arrowhead: F-actin cable; open arrowhead: MT). Disrupting F-actin by Latrunculin A treatment did not affect the MTs and disruption of MTs with the fungal-specific MT inhibitor Benomyl (Fuchs *et al*, 2005) did not disturb the F-actin organization (Supplementary Figure S1). These data suggest that F-actin and MTs function as independent tracks for polar delivery of secretory vesicles.

Filamentous fungi contain four classes of myosins (Steinberg, 2007). Out of these, class V myosin is a good candidate for vesicular transport. Previous work has shown that myosin-5 (Myo5) is involved in polarized hyphal growth in *U. maydis*, suggesting that it delivers secretory vesicles (Weber *et al*, 2003; Schuchardt *et al*, 2005). We tested the role of Myo5 and MTs in polarized growth by measuring the polarity index, which we define here as the ratio of cell length to cell width. Wild-type *U. maydis* cells were much longer than wide and had a polarity index of ∼7.8 (Figure 1D, control). Confirming previous results (Weber *et al*, 2003), we found that deletion of the *myo5* gene led to changes in cell morphology, including cell separation defects that led to the appearance of cell chains. However, the cells still maintained some polarity (Figure 1E, ΔMyo5, dotted arrows mark the axes), indicated by a polarity index of ∼3.3 (Figure 1D, ΔMyo5). We next asked if the ability to grow in a polarized fashion is due to the presence of MTs. We disrupted the MT array in ΔMyo5 mutants by treatment with Benomyl for 30 min. This led to a loss of the elongated cell shape (Figure 1E, ΔMyo5, + Benomyl) and the polarity index dropped to ∼1.5 (Figure 1D, ΔMyo5 + Ben). This suggested that both myosin-5 and MT-dependent motors contribute to

Table I Genotype of strains and plasmids used in this study

AB33GT	*a2* P*narbW2* P*narbE1 ble*^{R}/potefGFPTub1	Schuster *et al* (2011b)
AB33GLAct	*a2* P*narbW2* P*narbE1 ble*^{R}/poGLifeact	This study
AB33GLAct_ChTub1	*a2* P*narbW2* P*narbE1, ble*^{R}/poGLifeact/pHo$_m$ChTub1	This study
AB33ΔKin1	*a2* P*narbW2* P*narbE1* Δ*kin1::hyg*^{R} *ble*^{R}	Schuchardt *et al* (2005)
AB33ΔMyo5	*a2* P*narbW2* P*narbE1* Δ*myo5::hyg*^{R} *ble*^{R}	Schuchardt *et al* (2005)
AB33ΔMyo5rKin1	*a2* P*narbW2* P*narbE1* Δ*myo5::hyg*^{R} _P*crg-kin1 ble*^{R} *nat*^{R}	Schuchardt *et al* (2005)
FB1 Mcs1G$_3$	*a1 b1,* P*mcs1-mcs1-3xegfp hyg*^{R}	This study
FB1 Chs5G$_3$	*a1 b1,* P*chs5-chs5-3xegfp ble*^{R}	This study
FB1 Chs6G$_3$	*a1 b1,* P*chs6-chs6-3xegfp ble*^{R}	This study
SG200G$_3$Mcs1_mChSso1	*a1 mfa2 bW2 bE* Δ*mcs1::hyg*^{R} *ble*^{R}/pn3Mcs1/pomChSSO1	Treitschke *et al* (2010)
SG200G$_3$Mcs1	*a1 mfa2 bW2 bE* Δ*mcs1::hyg*^{R} *ble*^{R}/pn3Mcs1	Treitschke *et al* (2010)
AB5Dyn2^{ts}_Mcs1_3G	*a1*P*narbW2* P*narbE1* P*dyn2-dyn2*^{ts} P*mcs1-mcs1-3xegfp ble*^{R} *hyg*^{R} *nat*^{R}	This study
AB33ΔKin1_G$_3$Mcs1	*a2* P*narbW2* P*narbE1* Δ*kin1 ble*^{R} *hyg*^{R}/pn3Mcs1	This study
AB33 Mcs1G$_3$_rKin1^{rigor}	*a2* P*narbW2* P*narbE1* P*mcs1-mcs1-3xegfp ble*^{R} *hyg*^{R}/pNcrgKin1^{rigor}	This study
AB33 Mcs1G$_3$_mChTub1	*a2* P*narbW2* P*narbE1* P*mcs1-mcs1-3xegfp ble*^{R} *hyg*^{R}/po$_m$ChTub1	This study
AB33 Mcs1G$_3$_ rKin3^{rigor}_mChRab5a	*a2* P*narbW2* P*narbE1* P*mcs1-mcs1-3xegfp ble*^{R} *hyg*^{R}/ pcrgKin3^{G105E}/po$_m$ChRab5a	This study
AB33ΔKin3_mChRab5a_ G$_3$Mcs1	*a2* P*narbW2* P*narbE1* Δ*kin3 ble*^{R} *nat*^{R}/pHo$_m$ChRab5a/pn3Mcs1	This study
AB33G$_3$Myo5	*a2* P*narbW2* P*narbE1* P*myo5- 3xegfp-myo5, ble*^{R}, *hyg*^{R}	This study
AB33 Mcs1G$_3$_mCh$_3$Myo5	*a2* P*narbW2* P*narbE1* P*mcs1-mcs1-3xegfp* P*myo5-3xmCherry-myo5 ble*^{R} *hyg*^{R}, *nat*^{R}	This study
AB33G$_3$Myo5_mCh$_3$Mcs1	*a2* P*narbW2* P*narbE1* P*myo5- 3xegfp-myo5* P*mcs1-3xmCherry-mcs1 ble*^{R}, *hyg*^{R}, *nat*^{R}	This study
FB2ΔMyo5_G$_3$Mcs1	*a2 b2,* Δ*myo5 hyg*^{R}/pn3Mcs1	This study
AB33 Mcs1G$_3$_rM5^{rigor}	*a2* P*narbW2* P*narbE1* P*mcs1-mcs1-3xegfp ble*^{R} *hyg*^{R}/pcrgMyo5^{rigor}	This study
AB33 Mcs1G$_3$_rM5^{rigor}_mChSso1	*a2* P*narbW2* P*narbE1* P*mcs1-mcs1-3xegfp ble*^{R} *hyg*^{R}/pcrgMyo5^{rigor}/pomChSSO1	This study
AB33G$_3$Dyn2	*a2* P*nar-bW2* P*nar-bE1*, P*dyn2-3xegfp-dyn2, ble*^{R}, *hyg*^{R}	Lenz *et al* (2006)
AB33G$_3$Dyn2_Kin1^{rigor}	*a2* P*nar-bW2* P*nar-bE1*, P*dyn2-3xegfp-dyn2, ble*^{R}, *hyg*^{R}/pCcrgKin1 ^{rigor}	This study
AB33G$_3$Myo5_Kin1^{rigor}	*a2* P*narbW2* P*narbE1*, P*myo5- 3xegfp-myo5, ble*^{R}, *hyg*^{R}/pNcrgKin1 ^{rigor}	This study
SG200G$_3$Mcs1$^{\Delta MM}$	*a1 mfa2 bW2 bE* Δ*mcs1::hyg*^{R} *ble*^{R}/pn3GΔMM	Treitschke *et al* (2010)
SG200G$_3$Mcs1^{rigor}	*a1 mfa2 bW2 bE* Δ*mcs1::hyg*^{R} *ble*^{R}/pn3GMcs1^{rigor}	This study
SG200G$_3$Mcs1^{rigor}_mChSso1	*a1 mfa2 bW2 bE* Δ*mcs1::hyg*^{R} *ble*^{R}/pn3GMcs1^{rigor}/pomChSSO1	This study
SG200G$_3$Mcs1$^{\Delta MM}$_mChSso1	*a1 mfa2 bW2 bE* Δ*mcs1::hyg*^{R} *ble*^{R}/pn3GMcs1ΔMM/pomChSSO1	This study
potefGFPTub1	P*otef-egfp-tub1, cbx*^{R}	Steinberg *et al* (2001)
poGLifeact	P*otef-egfp-ABP140*$^{1-17\_modified}$ *cbx*^{R}	This study
pHo$_m$ChTub1	P*otef-mCherry-tub1, hyg*^{R}	This study
pomChSSO1	P*otef-mCherry-sso1 nat*^{R}	Treitschke *et al* (2010)
pn3GMcs1	P*mcs1-3xegfp-mcs1 cbx*^{R}	Treitschke *et al* (2010)
pNcrgKin1^{rigor}	P*crg-kin1*^{G96E} *nat*^{R}	This study
pCcrgKin1 ^{rigor}	P*crg-kin1*^{G96E}, *cbx*^{R}	This study
po$_m$ChTub1	P*otef-mCherry-tub1 cbx*^{R}	This study
po$_m$ChRab5a	P*otef-mcherry-rab5a, nat*^{R}	Schuster *et al* (2011a)
pHo$_m$ChRab5a	P*otef-mcherry-rab5a, hyg*^{R}	This study
pcrgKin3^{G105E}	P*crg-kin3*^{G105E}, *cbx*^{R}	Wedlich-Söldner *et al* (2002b)
pcrgMyo5^{rigor}	P*crg-HA-myo5* ^{G183E} *cbx*^{R}	This study
pcrgHAMcs1HN	P*crg-HA-mcs1*$^{1-927}$ *cbx*^{R}	Treitschke *et al* (2010)
pn3GMcs1ΔMM	P*mcs-3xegfp-mcs1*$^{\Delta 57-753}$ *cbx*^{R}	Treitschke *et al* (2010)
pn3GMcs1^{rigor}	P*mcs-3xegfp-mcs1*^{G113E} *cbx*^{R}	This study
pET15bMcs1HN	P*T7lac-6xHis- mcs1*$^{1-878}$	This study
pET15bMcs1HN^{rigor}	P*T7lac-6xHis- mcs1*$^{1-878;G113E}$	This study

a, *b*, mating type loci; P, promoter; -, fusion; Δ, deletion; *hyg*^{R}, hygromycin resistance; *ble*^{R}, phleomycin resistance; *nat*^{R}, nourseothricin resistance; *cbx*^{R}, carboxin resistance; *crg*, conditional arabinose-induced promoter; *otef*, constitutive promoter; ^{ts}, temperature-sensitive allele; /, ectopically integrated; *E1*, *W2*, genes of the *b* mating type locus; *egfp*, enhanced green fluorescent protein; *mCherry*, monomeric red fluorescent protein; *sso1*, a syntaxin-like plasma membrane protein; *mcs1*, myosin-chitin synthase 1; *kin1*^{G96E}, rigor allele of kinesin1; *kin1*^{G105E}, rigor allele of kinesin3; *rab5a*, small endosomal Rab5-like GTPase; *tub1*, tubulin; Myo5: class V myosin; *HA*, hemagglutinin epitope tag; *mcs1*^{G113E}, rigor allele of Mcs1; *myo5* $^{943-1611}$, tail of Myo5; *myo5* ^{G183E}, rigorously binding Myo5; *mcs1*$^{1-927}$, first 927 amino acids of Mcs1; *mcs1*$^{\Delta 57-753}$, Mcs1 without motor domain; *mcs1*$^{1-878;G113E}$, Mcs1 motor domain with rigor point mutation; *His*, Histidine epitope tag; *T7lac*, promoter for expression of proteins in *Escherichia coli*; *ABP140*$^{1-17\_modified}$, amino acids 1–17 of actin-binding protein 140 from *S. cerevisiae*, modified for use in filamentous fungi.

polar asymmetry. Kinesin-1 is a ubiquitous membrane transporter that utilizes MTs to support polarized growth in *U. maydis* (Lehmler *et al*, 1997; Schuchardt *et al*, 2005). When either kinesin-1 was deleted or MTs were disrupted by Benomyl, cells became thicker, indicated by a reduced polarity index (Figure 1D, Benomyl and ΔKin1). We generated a double mutant in which kinesin-1 was depleted and *myo5* deleted (strain AB33ΔMyo5rKin1; Table I). Again, polarized growth was strongly affected (Figure 1E, ΔMyo5Kin1↓) and the polarity index dropped to ∼1.6 (Figure 1D, ΔMyo5Kin1↓).

These results suggested that F-actin/myosin-5 and MTs/kinesin-1 participate in polarized secretion of factors that help shaping the cell. Morphogenesis of fungal cells depends on the extracellular cell wall, which receives its strength from chitin, a β-(1→4)—linked polymer of *N*-acetylglucosamine that is produced by secreted CHSs (Ruiz-Herrera *et al*, 2002). Therefore, we speculated that the morphological phenotype

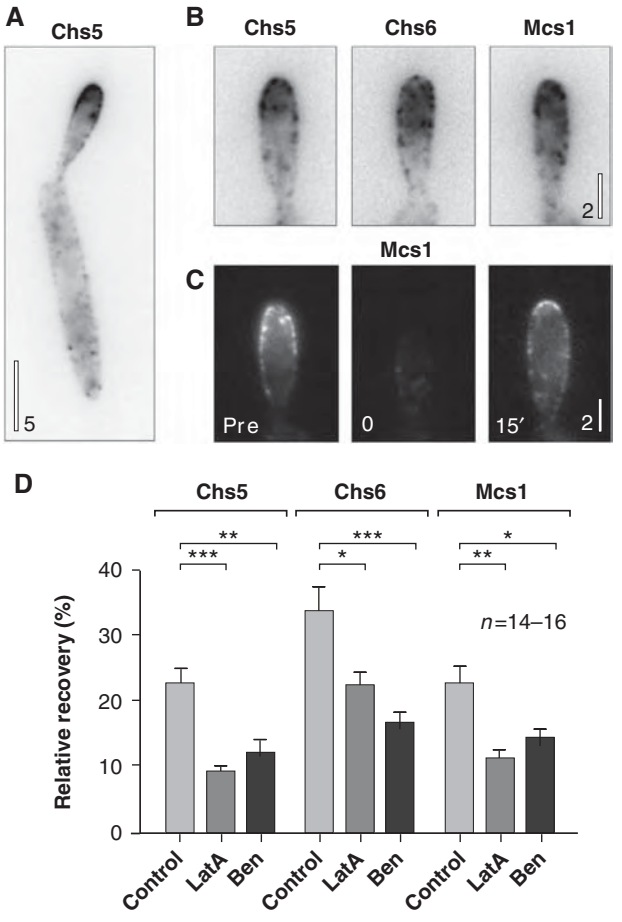

Figure 2 The role of the cytoskeleton in polar delivery of CHSs. (**A**) Localization of CHS5 in a yeast-like cell. Most of the CHS is concentrated at the growth region. Images are contrast inverted. Bar represents micrometers. (**B**) Polar localization of CHS5_G_3, CHS6_G_3 and Mcs1_G_3. The enzymes are located at the cell periphery, indicating that they get secreted into the plasma membrane where they participate in the formation of the cell-shaping extracellular cell wall. Images are contrast inverted. Bar represents micrometers. (**C**) Image series showing recovery of G_3Mcs1 signals after photo-bleaching at the growth region. Pre: prior to photo-bleaching, 0: immediately after the bleach, 15′: 15 min after photo-bleaching. Bar represents micrometers. (**D**) Bar chart showing recovery of apical fluorescence of CHS5_G_3, CHS6_G_3 and Mcs1_G_3 in cells treated with the solvent DMSO (control), the F-actin inhibitor Latrunculin A (LatA) or the MT inhibitor Benomyl (Ben). Note that CHS5 and MCS1 show a similar recovery behaviour, suggesting that they use similar delivery pathways. Statistical significance was tested using an unpaired *t*-test with Welch's correction. Single asterisk indicates statistical significance to control at $P<0.05$, double asterisks indicate statistical significance to control at $P<0.01$, and triple asterisks indicate statistical significance to control at $P<0.0001$. All bars are given as mean ± s.e.m., sample size n is indicated.

of motor mutants and drug-treated cells was due to defects in CHS secretion. *U. maydis* contains eight CHSs, and a subset of these localize to the growth region (Figure 2A and B; Weber *et al*, 2006). We performed fluorescent recovery after photo-bleaching (FRAP) experiments (Figure 2C) and monitored the recovery of triple-green fluorescent protein-tagged CHSs in the presence of inhibitors of the cytoskeleton. Indeed, we found that secretion of all tested CHSs depended on MTs and on F-actin (Figure 2D).

Mcs1-carrying secretory vesicles move bi-directionally

Filamentous fungi contain a unique type of CHS that contain an MMD at their N-terminus (Fujiwara *et al*, 1997) and are therefore also considered to be a class V CHS (Munro and Gow, 2001) as well as class 17 myosin (Hodge and Cope, 2000). The *U. maydis* myosin-17 (Mcs1; Weber *et al*, 2006) shares this domain organization (Figure 3A). Anterograde transport and subsequent insertion of the enzyme into the plasma membrane exposes the CHS region to the cell surface, which supports cell wall extension and plant infection (Treitschke *et al*, 2010). Previous work has shown that MTs and F-actin are involved in delivery of the Mcs1 (Treitschke *et al*, 2010). To visualize the delivery process, we fused a triple-green fluorescent protein to the N-terminus of the *mcs1* gene and expressed it under its own promoter in a *mcs1*-null mutant. The resulting fusion protein G_3Mcs1 was functional and rescued pathogenicity defects of *mcs1*-null mutants (Treitschke *et al*, 2010). In yeast-like cells that co-express a fusion of mCherry and the Sso1-like syntaxin (Treitschke *et al*, 2010), the G_3Mcs1-fusion protein concentrated in the plasma membrane of growing buds and along the lateral parts of the elongated mother cell (Figure 3B; Supplementary Figure S2). In addition, single G_3Mcs1 spots were found below the plasma membrane in the apical cortex, where they often remained stationary for several seconds (Supplementary Figure S2, right image series). In order to better visualize G_3Mcs1 motility, we photo-bleached the bud region using a 405-nm laser pulse (Figure 3C). We found individual G_3Mcs1 signals rapidly moving in the darkened area (Figure 3C; Supplementary Movie S2) in a bi-directional fashion. Again, G_3Mcs1 signals were seen that frequently paused near the cell cortex (Figure 3C, image series). This was best visible in kymographs, where movement of fluorescent particles appears as a series of diagonal lines, whereas stationary signals appear as vertical lines (arrowhead in Figure 3D). However, pausing only rarely led to membrane insertion (Figure 3E; Supplementary Movie S3) and ~85% of the signals returned to the cell centre without being exocytosed (Figure 3F; Supplementary Movie S4). We confirmed this result by FRAP experiments that demonstrated that Mcs1 secretion mainly occurred at the growth region, and, to a lower extent, along the sides of the bud and the mother cell (Figure 3G and H). G_3Mcs1 inserted into the plasma membrane remained stationary, even when the cortical F-actin was disrupted by the inhibitor Latrunculin A (Supplementary Figure S3), suggesting that secreted CHSs are anchored in the cell wall.

In *U. maydis*, MTs support bi-directional motility of early endosomes (EEs; Wedlich-Söldner *et al*, 2000; Schuster *et al*, 2011b) and we considered it possible that G_3Mcs1 travels in these organelles. To test this, we observed G_3Mcs1 in cells in which EE motility was abolished by (1) deleting the EE motor kinesin-3 and (2) expressing a kinesin-3 mutant protein that rigorously binds the organelles to the MTs ($Kin3^{rigor}$; Wedlich-Söldner *et al*, 2002b). In the absence of EE motility, G_3Mcs1 still concentrated at the growth region (Supplementary Figure S4A and B) and was normally secreted, as indicated by FRAP experiments (Supplementary Figure S4C, control versus ΔKin3 and $Kin3^{rigor}$; ANOVA testing: not significantly different, *P*:0.670). Furthermore, G_3Mcs1 moved at a mean velocity of 1.5 μm/s (anterograde and retrograde not different, *P*:0.6084), which was clearly slower than the rate

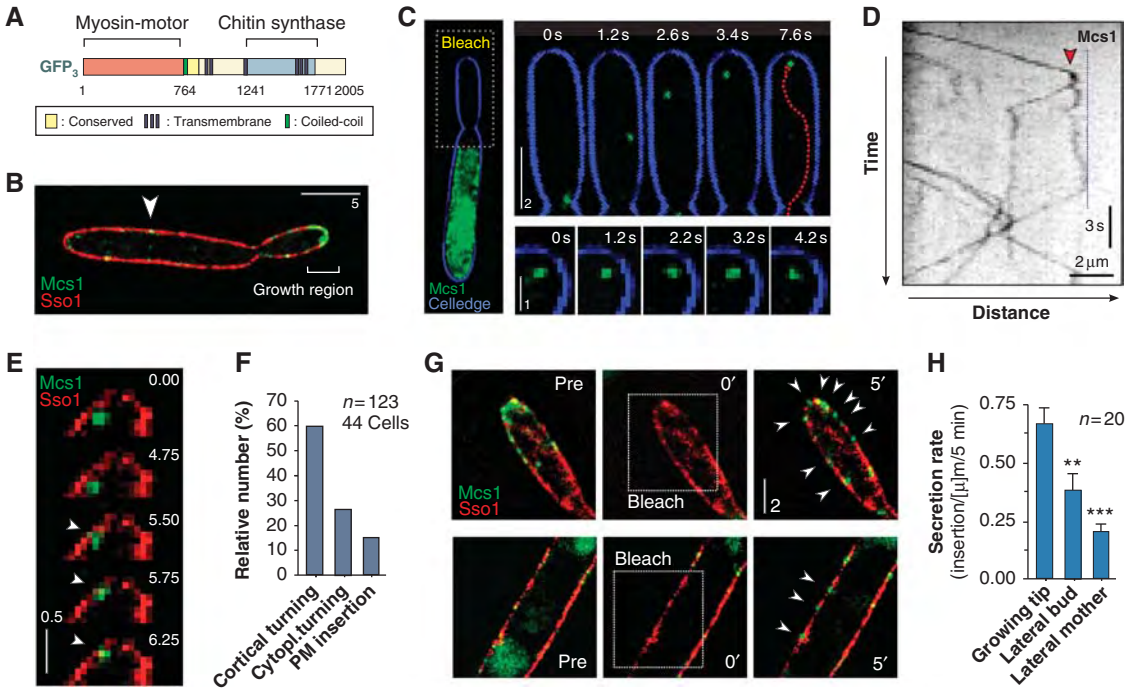

Figure 3 Motility behaviour of G_3Mcs1-bound secretory vesicles. (**A**) Domain organization of Mcs1 in *U. maydis*. The molecule contains an MMD and is therefore considered to be a member of the fungal-specific class 17 myosins. Its tail region contains a CHS domain that was shown to participate in formation of the extracellular cell wall (Treitschke *et al*, 2010). Myosin-17 motors are therefore also considered to be class V CHSs. (**B**) Localization of G_3Mcs1 (Mcs1) in yeast-like cells that co-express a syntaxin-like plasma membrane protein (Sso1) fused to mCherry. Note few G_3Mcs1 signals in the plasma membrane of the mother cell (arrowhead). Bar represents micrometers. (**C**) Motility of G_3Mcs1 (green) in a photo-bleached bud (bleach). G_3Mcs1 travels to the apex where it often rests for several seconds (image series). Cell edge is given in blue. Time is given in seconds; bar represents micrometers. See also Supplementary Movie S2. (**D**) Kymograph showing bi-directional motility of G_3Mcs1 in a bud that was photo-bleached (bleached). Signals often pause before they move back to the cell centre (left). Note that an anterograde signal splits in two after reaching the apical region (arrowhead). Time is given in seconds; distance is given in micrometers. The image was contrast inverted. (**E**) Image series showing pausing and subsequent insertion of a G_3Mcs1 signal (green) into the plasma membrane, labelled with the syntaxin-like Sso1 fused to mCherry (red). After long pausing, G_3Mcs1-bound vesicle gets in close proximity and eventually fuses with the plasma membrane (arrowheads). Time is given in seconds; bar represents micrometers. See also Supplementary Movie S3. (**F**) Bar chart showing the behaviour of Mcs1-carrying vesicles at the growing bud. Most vesicles reach the plasma membrane and turn around (cortical turning). Some signals are turning without contact with the plasma membrane (cytoplasmic turning). A minority gets inserted into the plasma membrane (membrane insertion). Total observation time is 1089.8 s. Sample size n is given. See also Supplementary Movie S4. (**G**) Image series showing recovery of G_3Mcs1 signals after photo-bleaching at the growth region (upper image series) and in the mother cell (lower image series). The plasma membrane is labelled by the syntaxin mCherry-Sso1 (red). Pre: prior to photo-bleaching, 0′: immediately after the bleach, 5′: 5 min after photo-bleaching. Bar represents micrometers. (**H**) Bar chart showing the recovery of G_3Mcs1 signals in the plasma membrane after local photo-bleaching. Statistical significance was tested using an unpaired *t*-test with Welch's correction. Double asterisks indicate statistical significance to control at $P<0.01$ and triple asterisks indicate significance to control at $P<0.0001$. All bars are given as mean ± s.e.m., sample size n is indicated.

of 1.9–2.2 µm/s previously reported for EE motility (Wedlich-Söldner *et al*, 2002b; Schuster *et al*, 2011a). We therefore considered it most likely that moving G_3Mcs1 signals are not located in EEs but indeed represent secretory CHS-containing vesicles (CSVs).

Vesicle motility depends on kinesin-1 and dynein

It was reported that in hyphal cells of *U. maydis*, long-range motility of G_3Mcs1 depends mainly on MTs (Treitschke *et al*, 2010), and the results described above confirm a role of MTs in secretion. In yeast-like cells, bi-directional long-range motility of G_3Mcs1-carrying vesicles could be observed (Figure 4A, arrowheads). This motility occurred along mCherry-labelled MTs (Supplementary Figure S5; Supplementary Movie S5) and was significantly impaired when MTs were disrupted by Benomyl (Figure 4B and C), suggesting that MTs support G_3Mcs1 motility.

In yeast-like cells, MTs have a uniform orientation with plus-ends directed towards the cell poles and minus-ends towards the mother-bud constriction (Straube *et al*, 2003). Thus, bi-directional motility within the photo-bleached buds indicated the participation of opposing motor systems (Figure 4B, MT orientation indicated with arrows). The best candidate for retrograde transport is cytoplasmic dynein, and we therefore investigated G_3Mcs1 motility in temperature-sensitive dynein mutants (Wedlich-Soldner *et al*, 2002a). Indeed, we found that motility of G_3Mcs1-bound vesicles was significantly impaired in these mutants (Figure 4C, $Dyn2^{ts}$). G_3Mcs1 still concentrated at the growth region, but formed apical cytoplasmic clusters (Figure 4D–F), suggesting that under normal conditions, dynein removes the excess of delivered CSVs. To address the mechanism of anterograde motility, we tested the role of the putative membrane transporter kinesin-1 in G_3Mcs1 motility. Deletion of *kin1* significantly reduced CSV motility (Figure 4C; Supplementary Movie S6) and drastically reduced Mcs1 accumulation at the growth region (Figure 4D–F). To confirm a direct role of kinesin-1 in delivery of CSVs, we expressed a mutant allele of kinesin-1 ($Kin1^{rigor}$) that, in previous work, has been shown

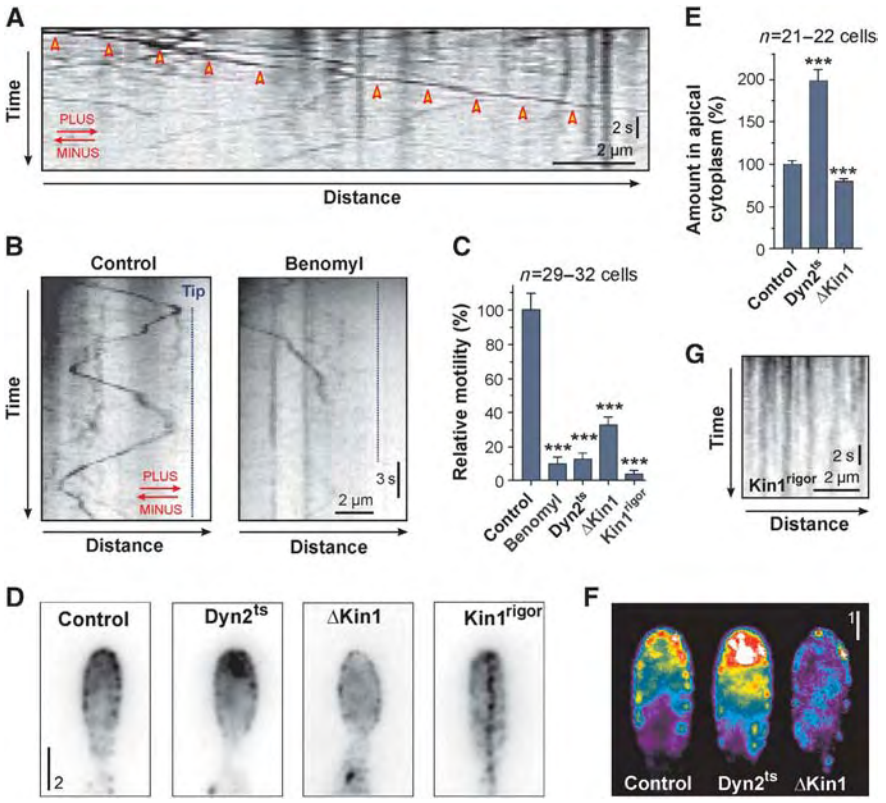

Figure 4 The role of MTs, kinesin-1 and dynein in motility of Mcs1-bound vesicles. (**A**) Kymograph showing anterograde long-range motility of G_3Mcs1-bound vesicles in a yeast-like cell. Arrowheads indicate long-range motility. Time is given in seconds; distance is given in micrometers. The image was contrast inverted. MT orientation is indicated in red. See also Supplementary Movie S6. (**B**) Kymographs displaying motility of G_3Mcs1 signals in photo-bleaching experiments. Bi-directional motility is almost abolished when MTs are disrupted (Benomyl). Time is given in seconds; distance is given in micrometers. The image was contrast inverted. MT orientation is indicated in red. (**C**) Bar chart showing G_3Mcs1 motility in control cells treated with the solvent DMSO (control) or the MT inhibitor Benomyl (Benomyl), and motility of G_3Mcs1 in temperature-sensitive dynein mutants ($Dyn2^{ts}$), kinesin-1-null mutants (ΔKin1) and kinesin-1 mutants that express a rigor allele ($Kin1^{rigor}$). Statistical significance was tested using an unpaired *t*-test with Welch's correction. Triple asterisks indicate statistical significance to control at $P<0.0001$. All bars are given as mean ± s.e.m., sample size *n* is indicated. (**D**) G_3Mcs1 localization in growing buds of control cells (control), in temperature-sensitive dynein mutants ($Dyn2^{ts}$), *kin1*-null mutants (ΔKin1) and mutants that express a *kin1* rigor allele ($Kin1^{rigor}$). Bar represents micrometers. Images were contrast inverted. See also Supplementary Movie S6. (**E**) Bar chart showing a quantitative analysis of the G_3Mcs1-signal intensity in the apical cytoplasm in control cells (control), a temperature-sensitive dynein mutant ($Dyn2^{ts}$) and a *kin1*-null mutant (ΔKin1). Statistical significance was tested using an unpaired *t*-test with Welch's correction. Triple asterisks indicate statistical significance to control at $P<0.0001$. All bars are given as mean ± s.e.m., sample size *n* is indicated. (**F**) False-coloured images of G_3Mcs1 at the growth region of control cells (control), a temperature-sensitive dynein mutant ($Dyn2^{ts}$) and a *kin1*-null mutant (ΔKin1). Note that the strong accumulation in $Dyn2^{ts}$ mutants is found beneath the plasma membrane. Bar represents micrometers. (**G**) Kymograph showing G_3Mcs1 signals in the presence of $Kin1^{rigor}$. Time is given in seconds; distance is given in micrometers. See also Supplementary Movie S6.

to bind rigorously to MTs (Straube *et al*, 2006). In the presence of $Kin1^{rigor}$, CSV motility was almost abolished (Figure 4C; Supplementary Movie S6), and immobile G_3Mcs1 particles were arranged in a pearl-string-like fashion along invisible tracks, which were most likely MTs (Figure 4D and G). Indeed, the G_3Mcs1 'pearl-strings' disappeared when MTs were disrupted by Benomyl. This suggests that the $Kin1^{rigor}$ protein anchored the G_3Mcs1-carrying vesicles to the MTs due to a physical interaction of kinesin-1 and the vesicles. Taken together, these data imply that long-range bi-directional motility of CSVs is based on MTs and is facilitated by the opposing motors dynein and kinesin-1.

Mcs1 motility involves F-actin and myosin-5

Deletion of kinesin-1 did not fully inhibit anterograde CSV motility (Figures 4C and 5A), and we found single vesicles moving independently of mCherry-MTs (Supplementary Movie S7). This suggested that another motor system participates in CSV delivery. The reported FRAP experiments suggested that secretion of Mcs1 involves F-actin (see above) and previous studies have shown that in hyphal cells of *U. maydis* motility of G_3Mcs1 signals is reduced when F-actin is destroyed (Treitschke *et al*, 2010). We therefore tested the possibility that the actomyosin system participates in vesicle motility. Indeed, when *kin1*-null mutants were treated with the F-actin inhibitor Latrunculin A, the residual CSV motility ceased (Figure 5A). This suggests that Mcs1-carrying secretory vesicles use F-actin and myosins for anterograde motility. *U. maydis* contains one class V myosin, Myo5, which was shown to be involved in polar cell growth and pathogenicity (Weber *et al*, 2003; Schuchardt *et al*, 2005). Class V myosins are vesicle transporters in several cell systems (Trybus, 2008), and Myo5 was therefore a good candidate for the actin-dependent transporter of CSVs. To investigate this possibility, we generated a strain in which the endogenous *myo5* gene was fused to triple-GFP. Most of the resulting G_3Myo5-expressing cells showed no severe morphological defects, indicating that the fusion protein is func-

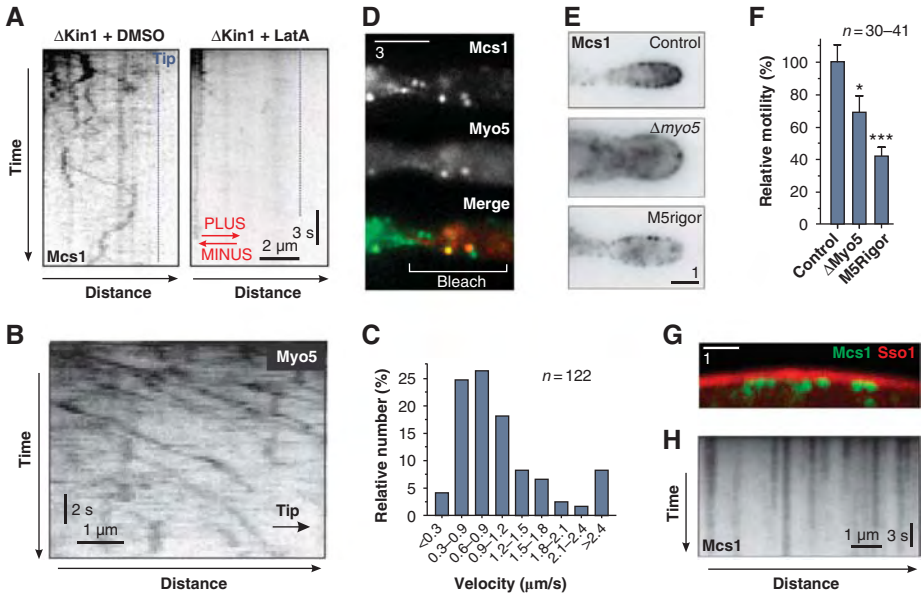

Figure 5 The role of F-actin and myosin-5 in motility of Mcs1-bound vesicles. (**A**) Kymographs showing motility of G_3Mcs1 in photo-bleached buds of *kin1*-null mutant cells treated with the solvent DMSO or the F-actin inhibitor Latrunculin A (LatA). Note that disruption of F-actin abolishes almost all residual motility. Time is given in seconds; distance is given in micrometers. The image was contrast inverted. MT orientation is indicated in red. (**B**) Kymograph showing motility of G_3Myo5. Note that the endogenous copy of *myo5* was tagged with triple-GFP. All signals move towards the growth region (indicated with arrow and 'Tip'). Time is given in seconds; distance is given in micrometers. The image was contrast inverted. See also Supplementary Movies S8 and S9. (**C**) Bar chart showing the velocity of G_3Myo5 motility. (**D**) Co-localization of G_3Mcs1 and mCh_3Myo5 in photo-bleached buds (bleach) of cells treated with 200 μM CCCP. Anterograde moving signals immobilize within the bud due to the reduction of ATP. Many stationary signals co-localize with fluorescent myosin-5. Bar represents micrometers. For co-localization of mCh_3Mcs1 and G_3Myo5, see also Supplementary Movie S10. (**E**) G_3Mcs1 in growing buds of control cells (control), in a *myo5*-null mutant (Δ*myo5*) and a mutant expressing a *myo5* rigor allele (M5rigor). Bars represent micrometers. Images were contrast inverted. (**F**) Bar chart showing G_3Mcs1 motility in control cells (control), in a *myo5*-null mutant (ΔMyo5) and in a mutant expressing a *myo5* rigor allele (M5Rigor). Statistical significance was tested using an unpaired *t*-test with Welch's correction. Single asterisk indicates statistical significance to control at $P<0.05$ and triple asterisks indicate significance to control at $P<0.0001$. All bars are given as mean ± s.e.m., sample size *n* is indicated. (**G**) G_3Mcs1 signals (green) at the periphery of a mutant expressing a *myo5* rigor allele and the syntaxin-like Sso1 fused to mCherry (red). Bar represents micrometers. (**H**) Kymograph of G_3Mcs1 signals at the periphery of a mutant expressing a *myo5* rigor allele. Time is given in seconds; distance is given in micrometers. Image was contrast inverted. See also Supplementary Movie S11.

tional. Consistent with previous reports (Weber *et al*, 2003), G_3Myo5 concentrated in the growing bud (Supplementary Movie S8). In addition, we found a continuous flow of faint G_3Myo5 signals along the cell periphery. This motility was directed towards the growth region (98.3% of the signal travelled towards the bud, $n=120$; Figure 5B; Supplementary Movies S8 and S9), with individual runs sometimes extending over 4–5 μm. This transport was inhibited when F-actin was disrupted using 20 μM Latrunculin A, suggesting that it occurs along the peripheral actin cables. While most signals moved at relatively low rates (Figure 5C), about one-third of all signals translocated at >1.2 μm/s, which corresponds well with the velocity of G_3Mcs1-bound vesicles (see above).

In order to test whether Myo5 localizes to Mcs1 vesicles, we used dual-colour imaging of G_3Mcs1 and a fusion protein of a triple monomeric Cherry fused to Myo5 (mCh_3Myo5). The mCh_3Myo5 signal was very faint and therefore was difficult to image at low exposure times. We therefore immobilized G_3Mcs1 vesicles by reducing cellular ATP levels using cyanide 3-chlorophenyl-hydrazone (CCCP). This method was previously used to investigate motor-cargo relation (Schuster *et al*, 2011b). Immobilized G_3Mcs1 signals often co-localized with mCh_3Myo5 (Figure 5D), supporting the notion that Myo5 participates in CSV delivery. Indeed, despite rapid bleaching of mCh_3Mcs1, co-transport with G_3Myo5 was occasionally visible in movies (Supplementary Movie S10). To test a role of Myo5 in CSV motility further, we investigated G_3Mcs1 localization and motility in a *myo5*-null mutant (ΔMyo5). In addition, we analysed CSV motility in cells expressing a *myo5*-allele containing a point mutation in the P-loop of the MMD (G183E; $Myo5^{rigor}$) that is expected to rigorously bind to F-actin (Sasaki and Sutoh, 1998). In both cases, the G_3Mcs1 accumulation at the growth region was abrogated (Figure 5E) and vesicle motility was significantly reduced (Figure 5F). Interestingly, expression of $Myo5^{rigor}$ immobilized CSVs and signals arranged at the periphery of the cells beneath the plasma membrane, where F-actin cables are located (Figure 5G, red: mCherry-Sso1; green: G_3Mcs1). The G_3Mcs1 signals remained stationary during the course of observation (Figure 5H; Supplementary Movie S11), indicating that $Myo5^{rigor}$ directly binds CSVs and tightly anchors them to the peripheral F-actin tracks. Indeed, when F-actin was disrupted by Latrunculin A, the G_3Mcs1 'pearl-strings' disappeared. This strongly suggests that G_3Mcs1-bound vesicles are a direct cargo of Myo5.

We next asked whether kinesin-1, dynein and myosin-5 bind to the same vesicle. If so, dynein and myosin-5 could be considered to be a passive cargo on kinesin-1 delivered vesicles. Consequently, we expected that expression of the $Kin1^{rigor}$ protein would immobilize GFP-tagged dynein or myosin-5 motors by anchoring the vesicles to the MTs. Indeed, motility of GFP_3-Dyn2 was blocked in the presence

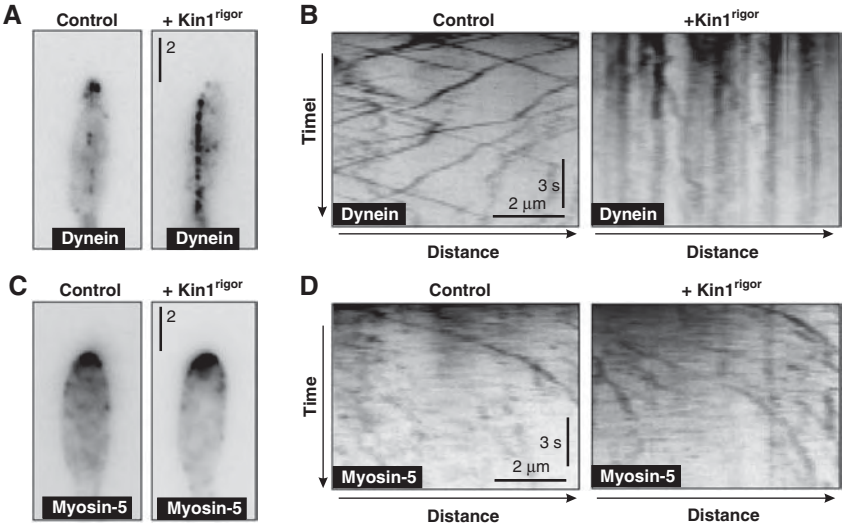

Figure 6 Motility of dynein and myosin-5 in Kin1^{rigor} mutants. (**A**) GFP-labelled dynein in control cells and in mutants expressing Kin1^{rigor}. Normally, dynein localizes along MTs and concentrates at MT plus-ends. After expression of Kin1^{rigor}, dynein decorates the MTs. Bar represents micrometers. (**B**) Kymograph showing the motility behaviour of G_3Dyn2 in control cells and in mutants expressing Kin1^{rigor}. When kinesin-1 tightly binds to MTs, dynein motility is abolished, suggesting a physical interaction between dynein and kinesin-1. Time is given in seconds; bar represents a micrometer. (**C**) GFP-labelled myosin-5 in control cells and in mutants expressing Kin1^{rigor}. In both conditions, the majority of G_3Myo5 concentrates at the growth region. Expression of Kin1^{rigor} did not anchor myosin-5 along the MTs. Bar represents micrometers. (**D**) Kymograph showing the motility behaviour of G_3Myo5 in control cells and in mutants expressing Kin1^{rigor}. Anchoring kinesin-1 to MTs did not abolish myosin-5 motility. Images were contrast inverted. Time is given in seconds; bar represents a micrometer.

of Kin1^{rigor} and dynein no longer concentrated at MT plus-ends, but instead was anchored as immobile dots along the central MTs (Figure 6A and B). However, expression of Kin1^{rigor} had no effect on motility or localization of G_3Myo5 (Figure 6C and D). This argues against a strong binding of myosin-5 to kinesin-1 delivered vesicle and instead suggests that two populations of vesicles exist, one travelling along F-actin, the other moving along MTs.

Myosin-17 transiently binds to F-actin but does not display motility

The results described so far strongly indicated that kinesin-1 and myosin-5 cooperate in CSV delivery. Mcs1 itself consists of a class 17 MMD fused to a CHS region (Weber *et al*, 2006). It was previously reported that the MMD has no role in long-range motility of the CSV to which it is bound (Treitschke *et al*, 2010), and we confirmed these results in yeast-like cells (Supplementary Figure S6). This raises the question of whether the MMD is able to bind to and move along F-actin. The MMD of Mcs1 shares only 22% sequence identity with Myo5 from *U. maydis* and 24% sequence identity with chicken myosin-2, suggesting that it might not function as a moving myosin-motor head. Nevertheless, it contained all functionally important regions, including (1) the nucleotide-binding regions GXXXXGKT/S (amino acid 108–115), LEAXGN (amino acid 151–157) and VNPY (amino acid 46–49); (2) the switch II region and relay helix that transmits motion from the catalytic site to the 'converter region' (amino acid 377–412); and (3) a less well-conserved light chain binding region (amino acid 629–695), suggesting that there is a canonical lever arm structure. We generated a comparative model of the MMD of Mcs1 that was based on published crystal structures of chicken smooth muscle myosin, chicken myosin-5a, squid muscle myosin and *Dictyostelium discoideum* myosin II (see Materials and methods). This revealed that Mcs1, despite its low sequence conservation, adopts a myosin-head domain fold (Figure 7A; Supplementary Movie S12). These results demonstrate that all the vital parts of an MMD are present in Mcs1.

We next asked whether the MMD of Mcs1 is able to interact with F-actin. To analyse this, we expressed recombinant 6 × His-tagged motor protein including parts of the neck region (His-Mcs1HN, amino acid 1–827) in an *in vitro* transcription–translation system. The Mcs1HN protein co-sedimented with F-actin in the absence of ATP (Figure 7B, Apyrase, P: pellet), but when 5 mM ATP was added, the protein remained soluble in the supernatant (Figure 7B, + ATP, S: supernatant). This suggests that the myosin-17 MMD behaves like other myosins that bind and release from F-actin in an ATP-dependent manner. However, the truncated MMD protein showed a tendency to aggregate (Treitschke *et al*, 2010), which made this assay less reliable. We therefore set out to obtain additional evidence for F-actin interaction using full-length Mcs1 protein. Due to the transmembrane domains in the C-terminal CHS domain, full-length Mcs1 is membrane bound, and hence co-sedimentation assays are unsuitable. Therefore, we visualized the interaction of Mcs1 with F-actin in a microscopic approach using *in vitro* binding assays and total internal reflection fluorescence microscopy. In these experiments, F-actin was immobilized on the surface of cover slips and partially purified and salt-stripped G_3Mcs1-bound membranes were added. In the presence of 3 mM ATP, G_3Mcs1 transiently bound to F-actin (Figure 7C–E, control, + ATP). However, no motility was detected (Figure 7F; Supplementary Movie S13). Instead, G_3Mcs1 membranes remained bound to F-actin for ∼7 s (7.1 ± 5.7 s, $n = 164$; ranging from ∼2 → 18 s; Figure 7F and G). The number of G_3Mcs1 signals interacting with actin filaments increased when ATP was depleted by apyrase treatment (Figure 7C and D, noATP). In contrast, almost no F-actin decoration was

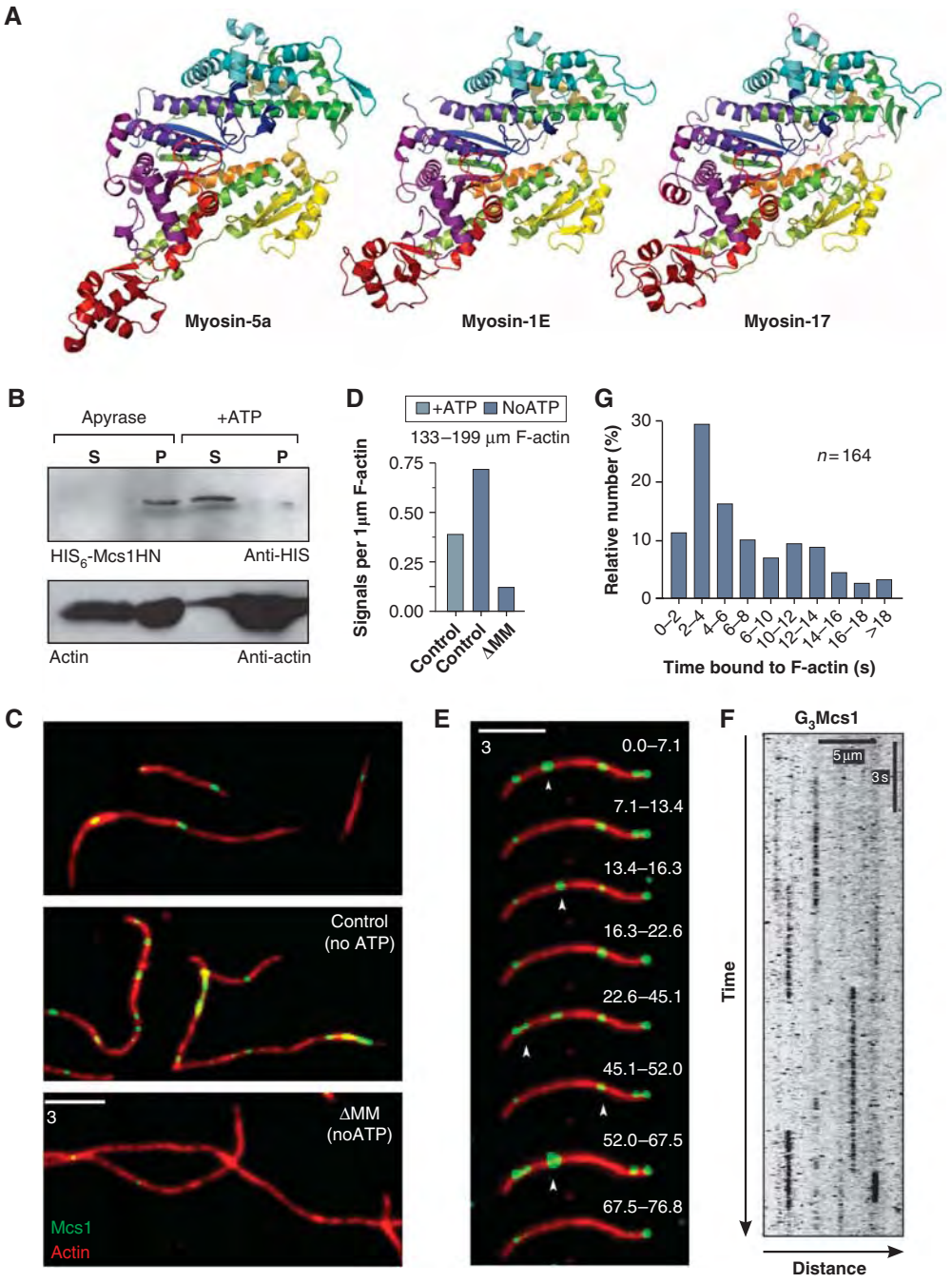

Figure 7 Mcs1 interacts with F-actin *in vitro* but no motility is performed. (**A**) Comparison of the MMD of chicken myosin V (myosin-5a), a *Dictyostelium* class I myosin (myosin-1E) and the comparative model of the MMD of Mcs1 (myosin-17). Images are coloured from blue (N-terminus) to red (C-terminus), with equivalent colours representing homologous sections of the protein. See also Supplementary Movie S12. (**B**) *In vitro* co-sedimentation of a truncated Mcs1 protein lacking the transmembrane domains and the CHS region (HIS_6-Mcs1HN, green) with F-actin (actin, red). Binding of the Mcs1 head to F-actin is ATP dependent. (**C**) *In vitro* observation of G_3Mcs1 (control) and $G_3Mcs1^{\Delta MM}$ (ΔMM) (green) bound to F-actin (red) in the presence (+ATP) and the absence of ATP (noATP). (**D**) Bar chart showing the average number of Mcs1 signals bound to 1 µm F-actin in the presence of 3 mM ATP (+ATP) or after apyrase treatment (noATP). (**E**) Image series showing transient binding of G_3Mcs1 (green) to F-actin (red). Images are the sum of all frames in the indicated time interval, given in seconds. See also Supplementary Movie S13. (**F**) Kymograph showing G_3Mcs1 behaviour in *in vitro* assays. Image was contrast inverted. Bars represent seconds and micrometers. (**G**) Bar chart showing binding times of G_3Mcs1 on F-actin.

found when the MMD was deleted (Figure 7C and D, ΔMM, noATP). These results confirmed that the myosin-17 MMD of Mcs1 reversibly binds to F-actin in an ATP-dependent manner. However, no directed motility of the myosin-17 was observed.

Myosin-17 tethers Mcs1-carrying vesicles at the apical growth region

CSVs normally paused at the growth region before they either returned to the cell centre or fused with the plasma membrane (see above; Figure 8A, control, red arrow). In control

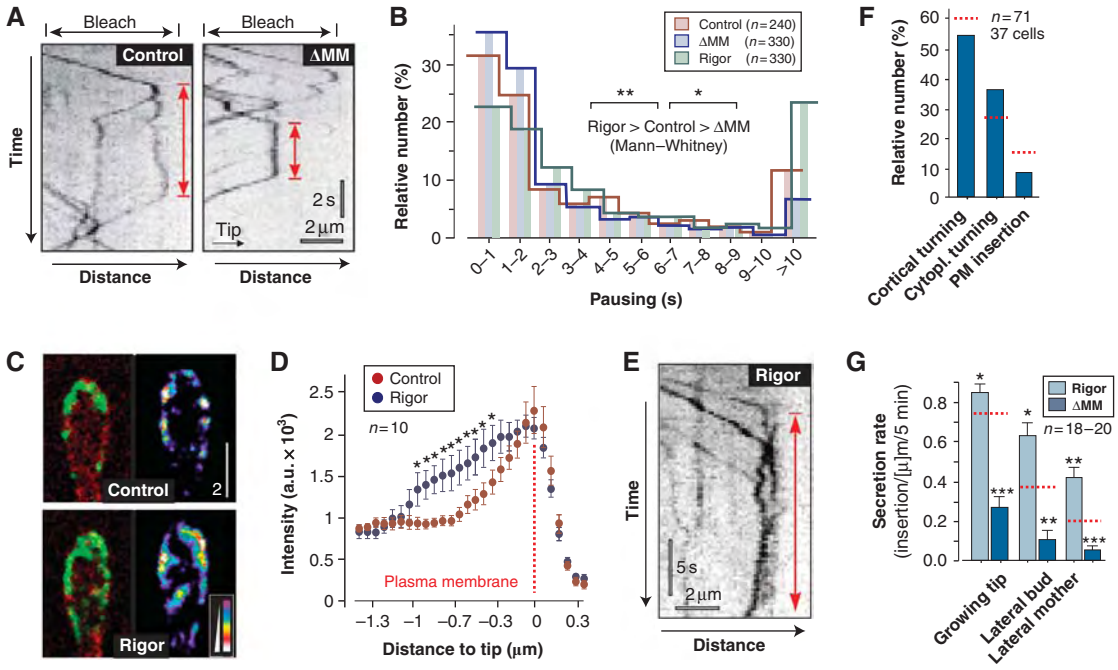

Figure 8 The MMD of Mcs1 controls apical residence time of Mcs1-bound vesicles. (**A**) Kymographs showing motility of G_3Mcs1 (control) and G_3Mcs1$^{\Delta MM}$ (ΔMM) in photo-bleached buds. In both strains, arriving vesicles pause (red arrows). Time is given in seconds; distance is given in micrometers. The images were contrast inverted. (**B**) Graph showing the apical residence time for G_3Mcs1 (control), the MMD truncated G_3Mcs1$^{\Delta MM}$ (ΔMM) and a rigorously binding mutant protein G_3Mcs1^{rigor} (rigor). Statistical significance was tested using an unpaired *t*-test with Welch's correction. Single asterisk indicates statistical significance to control at $P<0.05$ and double asterisks indicate statistical significance to control at $P<0.01$. All bars are given as mean ± s.e.m., sample size *n* is indicated. (**C**) Images of G_3Mcs1 in buds in control cells and cells expressing a fluorescent *mcs1* rigor protein (rigor). In control cells, G_3Mcs1 (left panel, green) localizes predominantly in the plasma membrane (mChSso1, red). In mutants, G_3Mcs1^{rigor} is also concentrated at the cortical cytoplasm (left panel, rigor). This localization is best visible in false-coloured images, where signal intensities are represented by colours (right panels). Bar represents micrometers. (**D**) Graph showing average signal intensity profiles for cells expressing either G_3Mcs1 (control) or G_3Mcs1^{rigor} (rigor). Statistical significance was tested using an unpaired *t*-test with Welch's correction. Asterisks indicate statistical significance to control at $P<0.05$. All bars are given as mean ± s.e.m., sample size *n* is indicated. (**E**) Kymographs showing motility of G_3Mcs1^{rigor} (rigor) in photo-bleached buds. Red arrow indicates pausing. Time is given in seconds; distance is given in micrometers. Image was contrast inverted. (**F**) Bar chart showing the behaviour of Mcs1-carrying vesicles at the growing bud in mutants that lack the myosin-17 MMD. Most vesicles turn around ('cortical turning' and 'cytoplasmic turning'). Only few signals were inserted into the plasma membrane (membrane insertion). Control values are indicated with dotted red lines (see Figure 3F). Note that compared with control cells, the secretion rate in ΔMM cells is reduced by ~40%. Sample size *n* is given. (**G**) Bar chart showing the recovery of G_3Mcs1$^{\Delta MM}$ (ΔMM) and G_3Mcs1^{rigor} (rigor) signals in the plasma membrane after local photo-bleaching. Statistical significance was tested using an unpaired *t*-test with Welch's correction. Single asterisk indicates statistical significance to control (see Figure 3H and dotted red lines) at $P<0.05$, double asterisks indicate statistical significance to control at $P<0.01$, and triple asterisks indicate statistical significance to control at $P<0.0001$. All bars are given as mean ± s.e.m., sample size *n* is indicated. Note that tightly binding of G_3Mcs1^{rigor} to cortical actin increases secretion, suggesting that Mcs1 tethers vesicles at the plasma membrane rather than transporting them along cortical actin.

cells, vesicles paused for ~4 s (3.9 ± 5.3 s, $n=240$; Figure 8B, control). Pausing of CSVs was also found when the MMD of Mcs1 was deleted (Figure 8A, ΔMM, red arrow), but the residence time was significantly shorter (Figure 8B, ΔMM; 2.9 ± 4.4 s, $n=330$; Mann–Whitney test, $P=0.0366$). This suggested that the MMD of Mcs1 facilitates tethering of CSVs to sites of exocytosis. To test this further, we generated a G_3Mcs1-allele carrying a point mutation G113E in the P-loop of the MMD (G_3Mcs1^{rigor}). Similar to the previous described Myo5^{rigor}, this mutant protein is expected to bind tightly to F-actin at the site of myosin-17 activity. Indeed, pull-down assays of a mutant protein carrying this point mutation confirm rigorous F-actin binding in the presence of ATP (Supplementary Figure S7). When expressed in *U. maydis mcs1*-null mutants, G_3Mcs1^{rigor} concentrated at the growth region, but in comparison to the control protein G_3Mcs1 accumulated beneath the plasma membrane near the growth region (Figure 8C, right images indicate intensity in pseudo-colours). Quantitative line-scan analysis confirmed this finding and revealed that significantly more G_3Mcs1^{rigor} than G_3Mcs1 protein localizes beneath the apical plasma membrane (Figure 8D, asterisk indicates significant difference at $P<0.05$). G_3Mcs1^{rigor}-carrying CSVs still underwent retrograde motility, but showed a significantly extended residence time at the apex (Figure 8B and E; $P=0.003$, Mann–Whitney test), which was most obvious for pauses longer than 10 s. The concentration of the immobile G_3Mcs1^{rigor} did result in a significant increase in secretion, as measured in FRAP experiments (Figure 8G, rigor red dotted lines represents wild-type levels). This argues against a function of the MMD in short-range motility, but supports the notion that the apical tethering fosters exocytosis of CSVs. Such a role in secretion is further supported by the observation that without the MMD (1) less vesicles insert in the plasma membrane (control: 14.8%, ΔMM: 8.5%; Figure 8F) and that (2) secretion is impaired (Figure 8G, ΔMM). In summary, these results suggest that CSVs are delivered to the growth region by kinesin-1 and myosin-5, whereas

dynein moves the vesicles back to the cell centre. Myosin-17 counteracts this retrograde motility by tethering vesicles to the site of exocytosis, thereby increasing their residence time and fostering exocytosis.

Discussion

MTs and F-actin provide independent routes for secretion

Live cell imaging of fluorescently labelled F-actin and MTs in *U. maydis* revealed that both filamentous systems could serve as tracks for delivery of vesicles to the growth region. Disrupting either of these filament systems did not severely affect the other and both localize in different regions in the cell. This demonstrates that F-actin and MTs form independent routes for membrane trafficking. The presence of F-actin cables in fungi and plants implies the use of myosin-5 in secretion (Woolner and Bement, 2009). Indeed, myosin-5 is required for polarized growth in *U. maydis* (Weber *et al*, 2003; Schuchardt *et al*, 2005), and we show here that myosin-5 motors continuously flow towards the growth region. This strengthens the notion that peripheral actin cables support polarized secretion. In *U. maydis*, MTs and associate motors have been shown to support bi-directional motility of EEs (Wedlich-Söldner *et al*, 2000; Lenz *et al*, 2006; Schuster *et al*, 2011b). However, inhibition of endosome transport did not affect cell morphology, but led to defects in cell–cell separation (Wedlich-Söldner *et al*, 2002b). Furthermore, polarized growth of *U. maydis* depends on the putative secretory motors myosin-5 and kinesin-1, a result that confirms previous reports in hyphal cells (Schuchardt *et al*, 2005). This suggests that MTs and F-actin cooperate in polarized secretion and morphogenesis. This conclusion gains further support from our photo-bleaching experiments that demonstrate that the apical recovery of CHSs depends on F-actin and MTs. The simplest explanation is that both cytoskeletal elements support growth by providing tracks for delivery of secretory vesicles.

Myosin-5 and kinesin-1 deliver a CHS to the growth region

We have shown that both kinesin-1 and myosin-5 participate in secretion of a CHS. Cooperation between myosin and kinesin motors in membrane trafficking is a common phenomenon (Brown, 1999). Most studies to date indicate that in animal cells, MTs and associated motors mediate long-range transport, whereas myosin-5 is supposed to be a short-range motor that supports motility in MT-free regions of the cell, such as the cellular cortex (Langford, 1995). In animal cells, kinesin-1 and myosin-5 directly interact (Huang *et al*, 1999; Stafford *et al*, 2000), suggesting that both motors are attached to the same vesicle. This allows individual organelles to use both MTs and F-actin, which was shown in extruded squid axoplasm (Kuznetsov *et al*, 1992, 1994) and melanosome motility within frog pigment cells (Gross *et al*, 2002). Myosin-5 and dynein also bind to the same organelles and their interplay controls organelle motility and distribution within the cell. Our results indicate that Mcs1, myosin-5, dynein and kinesin-1 cooperate in CSV delivery and secretion, which raises the possibility that these motors all co-localize on the vesicles. Indeed, the observation that rigorously binding kinesin-1 tightly anchors dynein to MTs suggests a physical interaction between these motors. However, myosin-5 was not immobilized in Kin1^{rigor} mutant cells, which argues that myosin-5 is only weakly associated with the two MT motors. This suggests that Mcs1 travels in two distinct classes of vesicles that travel along F-actin and along MTs. It is currently not clear if these are distinct populations of vesicles or whether the CSVs switch between both transport processes. Further studies are needed to provide insight into the nature of these vesicles.

Myosin-17 has a role in docking exocytic vesicles

Secretion is a directed process by which Golgi-derived vesicles are delivered to the cell periphery and exocytosed. In fungi, the cell wall is synthesized at the expanding cell pole and polarized secretion of cell wall-forming enzymes, such as CHS, is an essential requirement for tip extension during invasive growth. We show here that only 15% of the delivered CSVs become inserted into the plasma membrane. The remaining 85% fail to fuse and are recycled back towards the cell centre. While this behaviour is surprising, it is also found in animal cells (Nakata *et al*, 1998; Toonen *et al*, 2006) in which the majority of vesicles that reach the target membrane are not retained (residence time of <1 s). Successful exocytosis requires capture of the vesicles and extended tethering at the plasma membrane (>10 s) (Toonen *et al*, 2006; Verhage and Sorensen, 2008), which in animals involves the Sec1/Munc18-1 protein and the interaction with a t-SNARE (Toonen *et al*, 2006). The CSVs show a similar behaviour: the majority of the arriving vesicles pause for <2 s before dynein takes them back towards minus-ends; while some vesicles pause for >10 s. Although *U. maydis* contains a Sec1/Munc18-1 homologue (um11738, *P*:3.5e–85), our results suggest that filamentous fungi have developed a new retention mechanism that is based on the MMD of their myosin-CHSs. Several lines of evidence support a role of myosin-17 in vesicle docking: (1) deletion of the MMD of Mcs1 did not affect motility of CSVs, but significantly reduced the retention time and affected secretion; (2) a point mutation into the myosin-17 MMD that confers rigorous binding to actin significantly increased the CSV retention time and fostered secretion; and (3) in cell-free assays, the MMD of Mcs1 confers transient binding of CSVs but not directed motility. However, it needs to be considered that motility of myosin-17 might be very slow under *in vitro* conditions, but faster in the living cell, thereby supporting exocytosis by short-range motility near the plasma membrane. If this is the case, we would expect to see a decrease in secretion of Mcs1^{rigor}, as this mutant protein is immobile but accumulates at the growth region. However, in FRAP secretion assays, we do find a significant increase in Mcs1^{rigor} recovery after photo-bleaching. This result argues against a role as a short-range motor.

Previous work has shown that the ATPase activity and actin-binding capacity of myosin-17 is required for its function in CHS secretion (Treitschke *et al*, 2010). Thus, we consider it possible that myosin-17 captures CSVs by reversible binding to apical actin at the growth region. In animal cells, a similar mechanism might be supported by myosin-5. In enterochromaffin cells, vesicles pause prior to exocytosis. Silencing of myosin-5a reduced the residence time by $\sim$25%, which impairs secretion (Desnos *et al*, 2007). We found a similar decrease of vesicle retention time when the myosin-17

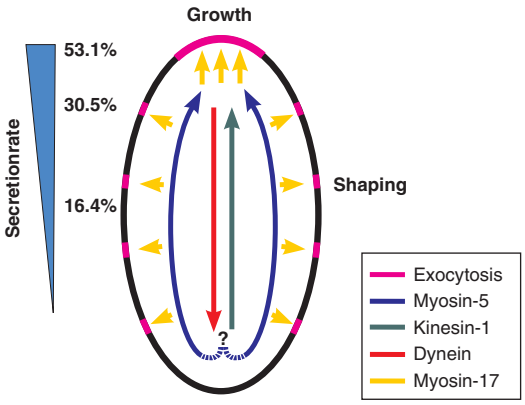

Figure 9 Model of the role of motors in CHS secretion. Kinesin-1 and myosin-5 take Mcs1-bound vesicles to the growth region, with myosin-5 walking along peripheral F-actin and kinesin-1 using more central MTs. Dynein takes over and moves them back towards the cell centre. Mcs1 interferes with this process by tethering the vesicle to the cortex, which fosters subsequent exocytosis. The combined activity of these motors generates a gradient of CHS secretion (relative secretion rate indicated with numbers). It is presently not clear if the same vesicle is transported along MTs and F-actin (indicated with '?').

MMD is deleted (24.5%; from 3.89 to 2.94 s). Thus, the moderate increase in CSV residence time by myosin-17 is sufficient to facilitate exocytosis.

Conclusion

Secretion of effector proteins and cell wall-forming enzymes is essential for virulence of plant pathogenic fungi (Panstruga and Dodds, 2009; Treitschke *et al*, 2010). We show here that secretion in the corn pathogen *U. maydis* involves two apparently independent routes (Figure 9). Peripheral actin cables support a continuous flow of myosin-5 towards the growth region. They also mediate lateral insertion of CHSs, suggesting that wall formation is not restricted to the growth region. In parallel, long-range transport of CSVs occurs along the more centrally located MTs. Our data argue that kinesin-1 and dynein are the underlying motors for this motility. The combined activity of all three motors mediates bi-directional motility of CSVs. Both, kinesin-1 and myosin-5 opposing retrograde dynein, which generates a net flow towards the expanding growth region. The MMD of Mcs1 most likely supports secretion by increasing the residence time of arriving vesicles. Such a local role of myosin-17 fits well in the emerging concept of unconventional myosins being dynamic tethers that cooperate with MTs (Loubery and Coudrier, 2008; Woolner and Bement, 2009). Class 17 myosins are only found in filamentous fungi where they contribute to virulence of numerous pathogens (Madrid *et al*, 2003; Liu *et al*, 2004; Weber *et al*, 2006; Werner *et al*, 2007). The knowledge of this fungal-specific exocytosis process promises the identification of novel fungicides required to ensure future crop security.

Materials and methods

Strains and plasmids

All plasmids were generated using standard techniques or *in vivo* recombination in *Saccharomyces cerevisiae* following published protocols (Raymond *et al*, 1999). Genotypes of all plasmids and strains are listed in Table I. Further details are described in the Supplementary data.

Growth conditions

All *U. maydis* cultures were grown overnight at 28 °C in complete medium (CM; Holliday, 1974; containing 1% (w/v) glucose), shaking at 200 revolutions per minute (r.p.m.). For induction of the *crg*-promoter, cells were grown in CM-glucose medium to an $OD_{600} = 0.5$ and transferred into CM containing 1% (w/v) arabinose as sole carbon source (CM-arabinose) and incubated for the indicated times at 28 °C, shaking at 200 r.p.m. Strain AB33ΔMyo5rKin1 was grown in CM containing 1% (w/v) arabinose. To repress the expression of Kin1, the cells were transferred into CM containing 1% (w/v) glucose for 12 h.

Sequence analysis and structural modelling

Sequence alignments were done using CLUSTALW (http://www.ebi.ac.uk/Tools/clustalw/index.html). Domain prediction was done at SMART server (http://smart.embl-heidelberg.de/). IQ-motif search was performed using the calmodulin target database (http://calcium.uhnres.utoronto.ca/ctdb/ctdb/sequence.html). Coiled-coil regions were predicted using the Coils2 server (http://www.ch.embnet.org).

Structural modelling of Mcs1 was based on published structures of myosins in the post-rigor conformation (chicken smooth muscle myosin, PDB ID: 2MYS, Rayment *et al*, 1993; chicken Myo5a, 1W7J, Coureux *et al*, 2004; squid muscle myosin, 2OY6, Yang *et al*, 2007; *D. discoideum* myosin II, 1MMD, Fisher *et al*, 1995). Sequence alignment was performed using CLUSTALW, followed by manual editing. Comparative models were prepared using MODELLER version 9.2 (Sali and Blundell, 1993). The best out of 10 models was selected on the basis of the MODELLER energy function, Ramachandran plot quality and conservation of secondary structure. Images were prepared using PyMOL (Schrödinger, New York, USA).

Laser-based epifluorescence microscopy

Microscopy was done essentially as previously described (Schuster *et al*, 2011a, b) using 488 and 562-nm solid-state lasers for excitation of fluorescent proteins. For FRAP experiments, cells were radiated by a 75-ms light pulse using a 405-nm laser (60 mW) at 100% laser power (beam diameter 30) and subsequent image series were taken. Kymographs were generated from the acquired image series using the MetaMorph software. Quantitative analysis of fluorescent intensities, velocities and flux-rates were done in raw 14-bit images or kymographs using MetaMorph. All statistical analyses were done using the software Prism 4 (GraphPad, La Jolla, CA, USA). Further details are described in the Supplementary data.

FRAP-based secretion assays

Secretion rates of CHSs were determined by taking reference images prior to photo-bleaching with a 405-nm light pulse. Image series were taken after 5–30 min and the recovery in the periphery of the cell was analysed. Stable insertion into the plasma membrane was confirmed in kymographs. Insertion rate was either defined as the average intensity per micrometer (CHSs secretion) or as the number of inserted signals per micrometer plasma membrane (secretion of G_3Mcs1 and G_3Mcs1^{rigor}). Further details are described in the Supplementary data.

Inhibitor experiments

For all inhibitor experiments, logarithmically growing cells were incubated for 30 min with either Benomyl at 30 μM (stock: 10 mM in DMSO; Fluka, Milwaukee, WI, USA) or Latrunculin A at 10 μM (stock: 20 mM in DMSO; kindly provided by Karen Tenney, University of California, Santa Cruz, USA). Control cells were treated with the respective amount of the solvent DMSO. Cells were placed onto a 2% agar cushion containing the respectively inhibitor and immediately observed.

Co-localization of Mcs1 and Myo5 under ATP depletion

To co-localize both proteins, cells of strain AB33 Mcs1G_3_Ch_3Myo5 were placed onto a 2% agar cushion containing 200 μM CCCP (carbonyl cyanide *m*-chlorophenyl-hydrazone; Sigma-Aldrich Ltd, Gillingham, UK). After photo-bleaching of the bud region of medium-sized budded cells, cells were incubated for 5 min and a dual image at 1000 ms exposure time was taken.

Actin co-sedimentation assay

Recombinant His-Mcs1H or His-Mcs1H^{rigor} was incubated with F-actin in buffer (20 mM Tris–HCl, pH 8.0, 5 mM $MgCl_2$ and 2 μM phalloidin) following the manufacturer's instructions (Cytoskeleton, Denver, USA). This was done in the presence of either 0.5 U apyrase (Sigma-Aldrich, Taufkirchen, Germany) or 5 mM ATP, respectively. After sedimentation of F-actin by centrifugation, the supernatant and pellet fractions were analysed by western blotting using an anti-His antibodies (Sigma-Aldrich, Taufkirchen, Germany).

Single molecule assays

Biotinylated and rhodamine-phalloidin-treated actin filaments were bound to neutravidin surfaces and placed in a flowcell. Partially purified and salt-stripped chitosomes carrying G_3Mcs1 or G_3Mcs1$^{\Delta MM}$ were incubated for 1–2 min at room temperature. Contaminating ATP was removed by apyrase treatment. The sample was illuminated using a totally internally reflected 532 or 488 nm laser. Fluorescence was imaged using the appropriate filters and an image intensified CCD camera (PTI-IC300, Ford, West Sussex, UK). Fluorescence break-through between channels was corrected by thresholding the eGFP signal above a critical value. Movies of 1000–1500 frames, taken at 25 f.p.s., were analysed using MetaMorph. All chemicals were sourced from Sigma-Aldrich (Gillingham, Dorset, UK). Further details are described in the Supplementary data.

Supplementary data

Supplementary data are available at *The EMBO Journal* Online (http://www.embojournal.org).

Acknowledgements

This work was supported by a grant from the BBSRC (BB/G00465X/1) and the DFG Graduate School 1216. The Max-Planck Institute for Terrestrial Microbiology in Marburg is acknowledged for providing equipment. We are grateful to Drs Regine Kahmann and Gunther Döhlemann, MPI Marburg, for providing laboratory space to ST. We thank Dr Uta Fuchs for providing the strains FB1 Mcs1G_3, FB1 Chs5G_3, Chs5G_3 and Ewa Bielska for providing strain AB33ΔKin3_mChRab5a. Professor Nick Talbot is gratefully acknowledged for discussion and Dr Magdalena Martin-Urdiroz for technical help. Finally, we thank the anonymous referees for their constructive criticism that significantly improved the manuscript. In particular, we are grateful for the suggestion that chitin synthase being leaked to the cell wall by the actin/myosin-5-dependent route.

Author contributions: MS generated strains, acquired microscopic data, designed some experiments and analysed the data; ST generated plasmids and strains and performed pull-down experiments; JM performed the *in vitro* motility assays and helped analysing sequence data; SK generated strains; NJH did the structural modelling; GS devised the project, designed the experiments, acquired and analysed the data and wrote the manuscript.

Conflict of interest

The authors declare that they have no conflict of interest.

References

Abramczyk D, Park C, Szaniszlo PJ (2009) Cytolocalization of the class V chitin synthase in the yeast, hyphal and sclerotic morphotypes of *Wangiella* (Exophiala) *dermatitidis*. *Fungal Genet Biol* **46:** 28–41

Allan VJ, Schroer TA (1999) Membrane motors. *Curr Opin Cell Biol* **11:** 476–482

Brown SS (1999) Cooperation between microtubule- and actin-based motor proteins. *Ann Rev Cell Dev Biol* **15:** 63–80

Coureux PD, Sweeney HL, Houdusse A (2004) Three myosin V structures delineate essential features of chemo-mechanical transduction. *EMBO J* **23:** 4527–4537

Desnos C, Huet S, Fanget I, Chapuis C, Bottiger C, Racine V, Sibarita JB, Henry JP, Darchen F (2007) Myosin va mediates docking of secretory granules at the plasma membrane. *J Neurosci* **27:** 10636–10645

Fisher AJ, Smith CA, Thoden JB, Smith R, Sutoh K, Holden HM, Rayment I (1995) X-ray structures of the myosin motor domain of Dictyostelium discoideum complexed with MgADP.BeFx and MgADP.AlF4. *Biochemistry* **34:** 8960–8972

Fuchs U, Manns I, Steinberg G (2005) Microtubules are dispensable for the initial pathogenic development but required for long-distance hyphal growth in the corn smut fungus *Ustilago maydis*. *Mol Biol Cell* **16:** 2746–2758

Fujiwara M, Horiuchi H, Ohta A, Takagi M (1997) A novel fungal gene encoding chitin synthase with a myosin motor-like domain. *Biochem Biophys Res Commun* **236:** 75–78

Gross SP, Tuma MC, Deacon SW, Serpinskaya AS, Reilein AR, Gelfand VI (2002) Interactions and regulation of molecular motors in *Xenopus* melanophores. *J Cell Biol* **156:** 855–865

Hodge T, Cope MJ (2000) A myosin family tree. *J Cell Sci* **113** (Part 19)**:** 3353–3354

Holliday R (1974) *Ustilago maydis*. In *Handbook of Genetics*, King RC (ed), **Vol. 1**, pp 575–595. New York: Plenum Press

Huang JD, Brady ST, Richards BW, Stenolen D, Resau JH, Copeland NG, Jenkins NA (1999) Direct interaction of microtubule- and actin-based transport motors. *Nature* **397:** 267–270

Kaksonen M, Sun Y, Drubin DG (2003) A pathway for association of receptors, adaptors, and actin during endocytic internalization. *Cell* **115:** 475–487

Kuznetsov SA, Langford GM, Weiss DG (1992) Actin-dependent organelle movement in squid axoplasm. *Nature* **356:** 722–725

Kuznetsov SA, Rivera DT, Severin FF, Weiss DG, Langford GM (1994) Movement of axoplasmic organelles on actin filaments from skeletal muscle. *Cell Motil Cytoskel* **28:** 231–242

Langford GM (1995) Actin- and microtubule-dependent organelle motors: interrelationships between the two motility systems. *Curr Opin Cell Biol* **7:** 82–88

Lehmler C, Steinberg G, Snetselaar KM, Schliwa M, Kahmann R, Bölker M (1997) Identification of a motor protein required for filamentous growth in *Ustilago maydis*. *EMBO J* **16:** 3464–3473

Lenz JH, Schuchardt I, Straube A, Steinberg G (2006) A dynein loading zone for retrograde endosome motility at microtubule plus-ends. *EMBO J* **25:** 2275–2286

Liu H, Kauffman S, Becker JM, Szaniszlo PJ (2004) *Wangiella* (*Exophiala*) *dermatitidis* WdChs5p, a class V chitin synthase, is essential for sustained cell growth at temperature of infection. *Eukaryot Cell* **3:** 40–51

Loubery S, Coudrier E (2008) Myosins in the secretory pathway: tethers or transporters? *Cell Mol Life Sci* **65:** 2790–2800

Madrid MP, Di Pietro A, Roncero MI (2003) Class V chitin synthase determines pathogenesis in the vascular wilt fungus *Fusarium oxysporum* and mediates resistance to plant defence compounds. *Mol Microbiol* **47:** 257–266

Munro CA, Gow NA (2001) Chitin synthesis in human pathogenic fungi. *Med Mycol* **39** (Suppl1)**:** 41–53

Nakata T, Terada S, Hirokawa N (1998) Visualization of the dynamics of synaptic vesicle and plasma membrane proteins in living axons. *J Cell Biol* **140:** 659–674

Panstruga R, Dodds PN (2009) Terrific protein traffic: the mystery of effector protein delivery by filamentous plant pathogens. *Science* **324:** 748–750

Rayment I, Rypniewski WR, Schmidt-Base K, Smith R, Tomchick DR, Benning MM, Winkelmann DA, Wesenberg G, Holden HM (1993) Three-dimensional structure of myosin subfragment-1: a molecular motor. *Science* **261:** 50–58

Raymond CK, Pownder TA, Sexson SL (1999) A general method for plasmid construction using homologous recombination. *Biotechniques* **26:** 134–141

Riedl J, Crevenna AH, Kessenbrock K, Yu JH, Neukirchen D, Bista M, Bradke F, Jenne D, Holak TA, Werb Z, Sixt M, Wedlich-Söldner R (2008) Lifeact: a versatile marker to visualize F-actin. *Nat Methods* **5:** 605–607

Ruiz-Herrera J, Gonzalez-Prieto JM, Ruiz-Medrano R (2002) Evolution and phylogenetic relationships of chitin synthases from yeasts and fungi. *FEMS Yeast Res* **1:** 247–256

Sali A, Blundell TL (1993) Comparative protein modelling by satisfaction of spatial restraints. *J Mol Biol* **234:** 779–815

Sasaki N, Sutoh K (1998) Structure-mutation analysis of the ATPase site of Dictyostelium discoideum myosin II. *Adv Biophys* **35:** 1–24

Schuchardt I, Assmann D, Thines E, Schuberth C, Steinberg G (2005) Myosin-V, kinesin-1, and kinesin-3 cooperate in hyphal growth of the fungus *Ustilago maydis*. *Mol Biol Cell* **16:** 5191–5201

Schuster M, Kilaru S, Ashwin P, Congping L, Severs NJ, Steinberg G (2011a) Controlled and stochastic retention concentrates dynein at microtubule ends to keep endosomes on track. *EMBO J* **30:** 652–664

Schuster M, Lipowsky R, Assmann MA, Lenz P, Steinberg G (2011b) Transient binding of dynein controls bidirectional long-range motility of early endosomes. *Proc Natl Acad Sci USA* **108:** 3618–3623

Stafford P, Brown J, Langford GM (2000) Interaction of actin- and microtubule-based motors in squid axoplasm probed with antibodies to myosin V and kinesin. *Biol Bull* **199:** 203–205

Steinberg G (2007) Hyphal growth: a tale of motors, lipids, and the Spitzenkorper. *Eukaryot Cell* **6:** 351–360

Steinberg G, Wedlich-Soldner R, Brill M, Schulz I (2001) Microtubules in the fungal pathogen Ustilago maydis are highly dynamic and determine cell polarity. *J Cell Sci* **114:** 609–622

Straube A, Brill M, Oakley BR, Horio T, Steinberg G (2003) Microtubule organization requires cell cycle-dependent nucleation at dispersed cytoplasmic sites: polar and perinuclear microtubule organizing centers in the plant pathogen *Ustilago maydis*. *Mol Biol Cell* **14:** 642–657

Straube A, Hause G, Fink G, Steinberg G (2006) Conventional kinesin mediates microtubule-microtubule interactions *in vivo*. *Mol Biol Cell* **17:** 907–916

Takeshita N, Ohta A, Horiuchi H (2005) CsmA, a class V chitin synthase with a myosin motor-like domain, is localized through direct interaction with the actin cytoskeleton in *Aspergillus nidulans*. *Mol Biol Cell* **16:** 1961–1970

Toonen RF, Wierda K, Sons MS, de Wit H, Cornelisse LN, Brussaard A, Plomp JJ, Verhage M (2006) Munc18-1 expression levels control synapse recovery by regulating readily releasable pool size. *Proc Natl Acad Sci USA* **103:** 18332–18337

Treitschke S, Döhlemann G, Schuster M, Steinberg G (2010) The myosin-motor domain of fungal chitin synthase V is dispensable for vesicle motility but required for plant pathogenicity. *Plant Cell* **22:** 2476–2494

Trybus KM (2008) Myosin V from head to tail. *Cell Mol Life Sci* **65:** 1378–1389

Vale RD (2003) The molecular motor toolbox for intracellular transport. *Cell* **112:** 467–480

Verhage M, Sorensen JB (2008) Vesicle docking in regulated exocytosis. *Traffic* **9:** 1414–1424

Weber I, Assmann D, Thines E, Steinberg G (2006) Polar localizing class V myosin chitin synthases are essential during early plant infection in the plant pathogenic fungus *Ustilago maydis*. *Plant Cell* **18:** 225–242

Weber I, Gruber C, Steinberg G (2003) A class-V myosin required for mating, hyphal growth, and pathogenicity in the dimorphic plant pathogen *Ustilago maydis*. *Plant Cell* **15:** 2826–2842

Wedlich-Söldner R, Bolker M, Kahmann R, Steinberg G (2000) A putative endosomal t-SNARE links exo- and endocytosis in the phytopathogenic fungus Ustilago maydis. *EMBO J* **19:** 1974–1986

Wedlich-Soldner R, Schulz I, Straube A, Steinberg G (2002a) Dynein supports motility of endoplasmic reticulum in the fungus *Ustilago maydis*. *Mol Biol Cell* **13:** 965–977

Wedlich-Söldner R, Straube A, Friedrich MW, Steinberg G (2002b) A balance of KIF1A-like kinesin and dynein organizes early endosomes in the fungus *Ustilago maydis*. *EMBO J* **21:** 2946–2957

Werner S, Sugui JA, Steinberg G, Deising HB (2007) A chitin synthase with a myosin-like motor domain is essential for hyphal growth, appressorium differentiation, and pathogenicity of the maize anthracnose fungus *Colletotrichum graminicola*. *Mol Plant Microbe Interact* **20:** 1555–1567

Woolner S, Bement WM (2009) Unconventional myosins acting unconventionally. *Trends Cell Biol* **19:** 245–252

Yang Y, Gourinath S, Kovacs M, Nyitray L, Reutzel R, Himmel DM, O'Neall-Hennessey E, Reshetnikova L, Szent-Gyorgyi AG, Brown JH, Cohen C (2007) Rigor-like structures from muscle myosins reveal key mechanical elements in the transduction pathways of this allosteric motor. *Structure* **15:** 553–564